Transp Porous Med (2011) 87:665–678
DOI 10.1007/s11242-010-9707-4

Linear Instability of the Isoflux Darcy–Bénard Problem in an Inclined Porous Layer

D. A. S. Rees · A. Barletta

Received: 26 November 2010 / Accepted: 22 December 2010 / Published online: 22 January 2011

Abstract The linear stability for convection in an inclined porous layer is considered for the case where the plane bounding surfaces are subjected to constant heat flux boundary conditions. A combined analytical and numerical study is undertaken to uncover the detailed thermoconvective instability characteristics for this configuration. Neutral curves and decrement spectra are shown. It is found that there are three distinct regimes between which the critical wavenumber changes discontinuously. The first is the zero-wavenumber steady regime which is well known for horizontal layers. The disappearance of this regime is found using a small-wavenumber asymptotic analysis. The second consists of unsteady modes with a nonzero wavenumber, while the third consists of a steady mode. Linear stability corresponds to inclinations which are greater than 32.544793° from the horizontal.

Keywords Porous media · Convection · Constant heat flux boundaries · Linear instability

1 Introduction

The first analyses which considered the onset of convection in a porous layer heated from below were by Horton and Rogers (1945) and Lapwood (1948). These authors considered the simplest possible configuration, namely an isotropic porous layer of infinite horizontal extent within which Darcy's law applies. Moreover, the Boussinesq approximation was taken to be valid and the solid, and fluid phases were in local thermal equilibrium. The lower impermeable surface was held at a uniform temperature which is above the uniform value corresponding to the upper surface, which is also impermeable. This is the porous analogue of the well known

D. A. S. Rees (✉)
Department of Mechanical Engineering, University of Bath, Claverton Down, Bath BA2 7AY, UK
e-mail: ensdasr@bath.ac.uk

A. Barletta
DIENCA, Alma Mater Studiorum, Università di Bologna, Viale Risorgimento 2, Bologna 40136, Italy
e-mail: antonio.barletta@unibo.it

and much older Rayleigh–Bénard problem. Thus, the present problem is often known as the Horton–Rogers–Lapwood problem, the Darcy–Bénard problem or just the porous Bénard problem. The criterion for the onset of convection for this classical problem is well known: the Darcy–Rayleigh number, Ra, must exceed $4\pi^2$ for convection to ensue, and the critical wavenumber is π.

The Darcy–Bénard problem has been studied in very great detail over the years, and lengthy reviews may be found in Rees (2000) and Tyvand (2002). It has also been developed in many directions even within the domain of linearised theory. Research has also covered weakly nonlinear theory, the computations of strongly nonlinear convection, and the onset of unsteady convection. In addition, extensions to Darcy's law have been included within the governing equations to determine how such non-Darcy effects alter the quantitative and qualitative nature of the stability properties. For example, the presence of conducting boundaries may yield cells with square planform at onset, rather than rolls (see Riahi 1983; Rees and Mojtabi 2010), while Bories and Combarnous (1973) report hexagonal planforms. The primary onset mode may in some circumstances become oscillatory, such as when the fluid is viscoelastic (Kim et al. 2003), or a when a second diffusing component, a solute, is present (Nield 1968). Other effects have been studied which are too numerous to list here.

However, relatively little is known when the bounding surfaces are subject to a constant heat flux whilst being heated from below and cooled from above. In the idealised situation of a domain of infinite extent, Nield (1968) shows that the critical parameters become $Ra = 12$ while the critical wavenumber is zero. Thus, the cells of square cross-section which correspond to fixed temperature boundary conditions are replaced by very long wavelength cells for constant heat flux boundaries. Kimura et al. (1995) extended the linear analysis of Nield (1968) to layers of finite extent in both horizontal directions, and provided computations of supercritical strongly nonlinear convection well into the unsteady regime. An interesting variation on this theme was provided by Mamou et al. (1998) who considered the effect of anisotropy on the onset of convection. They found that critical Darcy–Rayleigh number varies strongly with the anisotropy ratio, and that the critical wavenumber is no longer zero in general.

Our present interest lies in how the onset criterion changes when the layer is inclined at an angle to the horizontal. There exists two papers which present detailed numerical solutions for layers with constant heat flux boundary conditions, namely those by Vasseur et al. (1987) and Sen et al. (1987). The former concentrates on finite, but high aspect ratio cavities, and provides a careful comparison between a theoretical analysis based on a parallel flow approximation and fully nonlinear solutions. It was also shown that the number of cells which appear as a steady state solution depends not only on the Rayleigh number and the aspect ratio of the cavity, but also may depend on the form of the initiating disturbance. The latter paper extends this work and presents solutions which are anti-natural in the sense that the circulation of the cells are in a direction opposite to what might be expected on physical grounds.

Despite these detailed numerical studies, nothing is known about how the onset criterion changes for the idealised layer of infinite extent as the inclination increases from the horizontal towards the vertical. To this end we apply the various numerical schemes which were adopted in Rees and Bassom (2000) for the analogous layer with Dirichlet boundary conditions.

2 Governing Equations

We consider a fluid-saturated porous layer (see Fig. 1) of infinite extent which is inclined above the horizontal. The layer is heated from below and is thereby subject to thermoconvectve

Fig. 1 Inclined porous layer

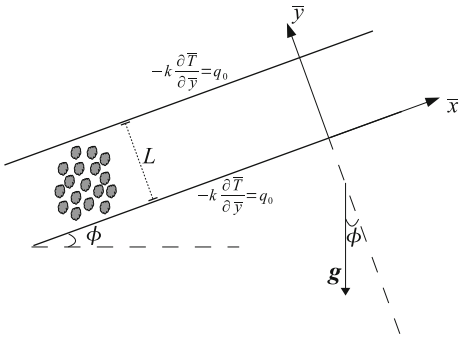

instability. Buoyancy-induced flow is described by assuming that Darcy's law and the Oberbeck–Boussinesq approximation are both valid, that the solid and fluid phases are in local thermal equilibrium, and that the effect of viscous dissipation is negligible. Thus, the local balance equations for mass, momentum and heat transport may be written in the form,

$$\overline{\nabla} \cdot \overline{\boldsymbol{u}} = 0, \tag{1}$$

$$\frac{\mu}{K}\,\overline{\boldsymbol{u}} = -\overline{\nabla}\,\overline{p} + \rho\, g\, \beta\left(\overline{T} - T_0\right)\left(\sin\phi\, \boldsymbol{e}_x + \cos\phi\, \boldsymbol{e}_y\right), \tag{2}$$

$$\sigma\frac{\partial \overline{T}}{\partial \overline{t}} + \overline{\boldsymbol{u}} \cdot \overline{\nabla}\,\overline{T} = \alpha\,\overline{\nabla}^2\,\overline{T}, \tag{3}$$

where $\overline{\boldsymbol{u}}$ is the Darcy velocity, $\overline{p}$ is the pressure, $\overline{T}$ is the temperature, μ is the dynamic viscosity, K is the permeability, ρ is the density, g is the modulus of the gravitational acceleration, β is the coefficient of thermal expansion, T_0 is the reference temperature, α is the average thermal diffusivity, σ is the ratio between the overall volumetric heat capacity of the porous medium and the volumetric heat capacity of the fluid.

The boundary planes of the porous layer, $\overline{y} = 0, L$, are impermeable. The lower plane at $\overline{y} = 0$ is heated with a uniform flux, $q_0 > 0$. This heat input is transferred entirely to the external environment through the upper boundary at $\overline{y} = L$, so that

$$\overline{y} = 0, L \;:\qquad \overline{v} = 0, \qquad -k\,\frac{\partial \overline{T}}{\partial \overline{y}} = q_0. \tag{4}$$

In the above equations the Cartesian components of $\overline{\boldsymbol{u}}$ have been denoted by $(\overline{u}, \overline{v}, \overline{w})$, while the unit vectors along the coordinate axes are $\left(\boldsymbol{e}_x, \boldsymbol{e}_y, \boldsymbol{e}_z\right)$. We note that the reference temperature T_0 which is used in the buoyancy force term in Eq. 2 does not appear explicitly in the boundary conditions, Eq. 4, and it is intended as the average temperature of the layer.

2.1 Dimensionless Quantities

The overline has been adopted to denote the dimensional velocity, pressure and temperature fields, the space and time coordinates and the differential operators. Equations 1–4 may be rendered dimensionless by defining the following scalings,

$$\begin{aligned}
\boldsymbol{x} = (x, y, z) &= \frac{1}{L}\,(\overline{x}, \overline{y}, \overline{z}) = \frac{1}{L}\,\overline{\boldsymbol{x}}, \quad t = \frac{\alpha}{\sigma\, L^2}\,\overline{t}, \\
\boldsymbol{u} = (u, v, w) &= \frac{L}{\alpha}\,(\overline{u}, \overline{v}, \overline{w}) = \frac{L}{\alpha}\,\overline{\boldsymbol{u}}, \quad T = \frac{\overline{T} - T_0}{q_0\, L}\,k.
\end{aligned} \tag{5}$$

Thus, we obtain

$$\nabla \cdot \boldsymbol{u} = 0, \tag{6}$$

$$\nabla \times \boldsymbol{u} = R\left[-\frac{\partial T}{\partial z}\cos\phi\,\boldsymbol{e}_x + \frac{\partial T}{\partial z}\sin\phi\,\boldsymbol{e}_y + \left(\frac{\partial T}{\partial x}\cos\phi - \frac{\partial T}{\partial y}\sin\phi\right)\boldsymbol{e}_z\right], \tag{7}$$

$$\frac{\partial T}{\partial t} + \boldsymbol{u}\cdot\nabla T = \nabla^2 T, \tag{8}$$

$$y = 0, 1: \qquad v = 0, \qquad \frac{\partial T}{\partial y} = -1. \tag{9}$$

Equation 7 was obtained by applying the curl operator to both sides of Eq. 2 to eliminate the pressure field. The governing dimensionless parameter,

$$R = \frac{\rho\, g\, \beta\, q_0\, K\, L^2}{\mu\, \alpha\, k}, \tag{10}$$

is the Darcy–Rayleigh number, where $q_0 L/k$ has been taken as the temperature scale.

2.2 The Basic Solution

The stationary solution of Eqs. 6–9 which has a zero mean flow in the x-direction is given by

$$u_{\mathrm{B}} = \frac{R}{2}(1-2y)\sin\phi, \quad v_{\mathrm{B}} = 0, \quad w_{\mathrm{B}} = 0, \quad T_{\mathrm{B}} = 1 - y, \tag{11}$$

where the subscript "B" stands for "basic solution".

3 Linear Disturbances

The basic solution is now subjected to small-amplitude disturbances of magnitude $\varepsilon \ll 1$ as given by,

$$\boldsymbol{u} = \boldsymbol{u}_{\mathrm{B}} + \varepsilon\,\boldsymbol{U}, \quad T = T_{\mathrm{B}} + \varepsilon\,\theta, \tag{12}$$

where $\boldsymbol{U} = (U, V, W)$. On substituting Eq. 12 into Eqs. 6–9, and keeping only those terms which are of $O(\varepsilon)$, we obtain the governing equations for the linear disturbances,

$$\nabla \cdot \boldsymbol{U} = 0, \tag{13}$$

$$\nabla \times \boldsymbol{U} = R\left[-\frac{\partial \theta}{\partial z}\cos\phi\,\boldsymbol{e}_x + \frac{\partial \theta}{\partial z}\sin\phi\,\boldsymbol{e}_y + \left(\frac{\partial \theta}{\partial x}\cos\phi - \frac{\partial \theta}{\partial y}\sin\phi\right)\boldsymbol{e}_z\right], \tag{14}$$

$$\frac{\partial \theta}{\partial t} + \frac{R}{2}(1-2y)\sin\phi\,\frac{\partial \theta}{\partial x} - V = \nabla^2\theta, \tag{15}$$

$$y = 0, 1: \qquad V = 0, \qquad \frac{\partial \theta}{\partial y} = 0. \tag{16}$$

The fate of rolls aligned at a general orientation, γ, to the x-direction may be determined by first introducing a coordinate rotation in the xz-plane so that the new coordinates are,

$$\widetilde{x} = x\,\cos\gamma + z\,\sin\gamma, \quad \widetilde{z} = -x\,\sin\gamma + z\,\cos\gamma, \tag{17}$$

while the new velocity components are,

$$\widetilde{U} = U\,\cos\gamma + W\,\sin\gamma, \quad \widetilde{W} = -U\,\sin\gamma + W\,\cos\gamma. \tag{18}$$

In the rotated frame, Eqs. 14 and 15 may be rewritten as

$$\nabla \times \boldsymbol{U} = R\left[\left(-\frac{\partial\theta}{\partial\widetilde{z}}\,\cos\phi - \frac{\partial\theta}{\partial y}\,\sin\phi\,\sin\gamma\right)\boldsymbol{e}_{\widetilde{x}} + \left(\frac{\partial\theta}{\partial\widetilde{x}}\,\sin\gamma + \frac{\partial\theta}{\partial\widetilde{z}}\,\cos\gamma\right)\right.$$
$$\left.\times\,\sin\phi\,\boldsymbol{e}_y + \left(\frac{\partial\theta}{\partial\widetilde{x}}\,\cos\phi - \frac{\partial\theta}{\partial y}\,\sin\phi\,\cos\gamma\right)\boldsymbol{e}_{\widetilde{z}}\right], \tag{19}$$

$$\frac{\partial\theta}{\partial t} + \frac{R}{2}\,(1-2\,y)\,\sin\phi\left(\frac{\partial\theta}{\partial\widetilde{x}}\,\cos\gamma - \frac{\partial\theta}{\partial\widetilde{z}}\,\sin\gamma\right) - V = \nabla^2\theta, \tag{20}$$

where $\boldsymbol{e}_{\widetilde{x}}$ and $\boldsymbol{e}_{\widetilde{z}}$ are the unit vectors along the $\widetilde{x}$-direction and the $\widetilde{z}$-direction, respectively. General oblique rolls are wavelike solutions endowed with a translational invariance along the $\widetilde{z}$-direction, namely,

$$\frac{\partial}{\partial\widetilde{z}}\,(\boldsymbol{U},\theta) = 0. \tag{21}$$

While a general $\gamma \in [0, \pi/2]$ describes oblique rolls, the choice $\gamma = 0$ defines transverse rolls (and hence convection remains two-dimensional), and $\gamma = \pi/2$ corresponds to longitudinal rolls.

By employing Eq. 21, the $\widetilde{x}$-and y-components of Eq. 19 are satisfied when,

$$\widetilde{W} = -\,R\,\theta\,\sin\phi\,\sin\gamma, \tag{22}$$

and

$$\frac{\partial V}{\partial\widetilde{x}} - \frac{\partial\widetilde{U}}{\partial y} = R\left(\frac{\partial\theta}{\partial\widetilde{x}}\,\cos\phi - \frac{\partial\theta}{\partial y}\,\sin\phi\,\cos\gamma\right), \tag{23}$$

while Eq. 13 is identically satisfied by defining a streamfunction ψ such that

$$\widetilde{U} = \frac{\partial\psi}{\partial y}, \quad V = -\frac{\partial\psi}{\partial\widetilde{x}}. \tag{24}$$

Therefore, the governing equations for the linear disturbances, 16, 20 and 23, subject to the condition Eq. 21, may be rewritten in the following temperature-streamfunction formulation,

$$\frac{\partial^2\psi}{\partial\widetilde{x}^2} + \frac{\partial^2\psi}{\partial y^2} = -R\left(\frac{\partial\theta}{\partial\widetilde{x}}\,\cos\phi - \frac{\partial\theta}{\partial y}\,\sin\phi\,\cos\gamma\right), \tag{25}$$

$$\frac{\partial\theta}{\partial t} + \frac{R}{2}\,(1-2\,y)\,\frac{\partial\theta}{\partial\widetilde{x}}\,\sin\phi\,\cos\gamma + \frac{\partial\psi}{\partial\widetilde{x}} = \frac{\partial^2\theta}{\partial\widetilde{x}^2} + \frac{\partial^2\theta}{\partial y^2}, \tag{26}$$

$$y = 0, 1 \;:\qquad \psi = 0, \qquad \frac{\partial\theta}{\partial y} = 0. \tag{27}$$

Equation 22 is not needed in the solution of Eqs. 25–27. Equation 22 shows that the oblique rolls, although invariant by translations in the $\widetilde{z}$-direction, are such that the velocity streamlines are winding lines in the $\widetilde{z}$-direction. These streamlines are the result of the combination of a multicellular flow in the $\widetilde{x}y$-plane and the drift flow described by Eq. 22 in the $\widetilde{z}$-direction. The drift flow component $\widetilde{W}$ vanishes either when the layer is horizontal ($\phi = 0$) or when the direction $\widetilde{z}$ of the translational invariance is orthogonal to the x-axis ($\gamma = 0$, i.e. transverse rolls).

Plane waves propagating in the $\widetilde{x}$-direction are expressed as

$$\psi = \Re\left(i\,f(y)\,e^{\lambda t}\,e^{i\,a\,\widetilde{x}}\right), \quad \theta = \Re\left(h(y)\,e^{\lambda t}\,e^{i\,a\,\widetilde{x}}\right), \tag{28}$$

where a is the wave number, a real quantity, and λ is the complex growth rate, while $\Re(\cdot)$ and $\Im(\cdot)$ denote the real part and the imaginary part. When $\Re(\lambda)$ is positive, then the magnitude of the disturbance grows exponentially in time and the basic state is unstable. On the other hand, we have stability for $\Re(\lambda) < 0$ and neutral stability for $\Re(\lambda) = 0$. We now substitute Eq. 28 into Eqs. 25–27, so that we obtain,

$$f'' - a^2 f + R\left(i h' \sin\phi \cos\gamma + a h \cos\phi\right) = 0, \tag{29}$$

$$h'' + \left[i a R\left(y - \frac{1}{2}\right)\sin\phi \cos\gamma - \lambda - a^2\right] h + a f = 0, \tag{30}$$

$$y = 0, 1: \qquad f = 0, \qquad h' = 0, \tag{31}$$

where the primes denote differentiation with respect to y.

Following the procedure described by Rees and Bassom (2000), we may define a transformed angle $\Phi \in [0, \pi/2]$ and a transformed Rayleigh number, S, using

$$\tan\Phi = \tan\phi \cos\gamma, \quad S = R\sqrt{\sin^2\phi \cos^2\gamma + \cos^2\phi}, \tag{32}$$

in order to reduce the number of nondimensional parameters by one. Thus, Eqs. 29–31 may be rewritten as

$$f'' - a^2 f + S\left(i h' \sin\Phi + a h \cos\Phi\right) = 0, \tag{33}$$

$$h'' + \left[i a S\left(y - \frac{1}{2}\right)\sin\Phi - \lambda - a^2\right] h + a f = 0, \tag{34}$$

$$y = 0, 1: \qquad f = 0, \qquad h' = 0. \tag{35}$$

Equations 33–35 are an alternative representation of the eigenvalue problem for general oblique rolls, Eqs. 29–31. They show that the solution of Eqs. 29–31 with an arbitrary γ is equivalent to the solution of the same system of ODEs with $\gamma = 0$, provided that the replacements $R \to S$ and $\phi \to \Phi$ are performed. This means that the solution of Eqs. 29–31 for an arbitrary γ can be always reduced to the solution for transverse rolls ($\gamma = 0$). This result was first used by Rees and Bassom (2000).

The representation of Eqs. 33–35 as an eigenvalue problem implies that, for every assignment of $(a,\ \Re(\lambda),\ \Phi)$, the eigenvalue pair $(\Im(\lambda),\ S)$ is determined through the solution of Eqs. 33–35. The ensuing analysis is focused on the solution of the eigenvalue problem for the condition of neutral stability, i.e. for $\Re(\lambda) = 0$.

We note that when the rolls are longitudinal ($\gamma = \pi/2$) then Eq. 32 yields $\Phi = 0$ and $S = R\cos\phi$. This means that the stability analysis for longitudinal rolls reduces to that of the horizontal case where $R\cos\phi$ plays the role of the Darcy–Rayleigh number. This has already been pointed out by Nield and Bejan (2006) for the classical case of Dirichlet boundary conditions, but it also applies here for Neumann boundary conditions. Therefore the stability criterion for longitudinal rolls is, simply,

$$R_{\rm cr} = 12/\cos\phi, \qquad a_{\rm cr} = 0 \tag{36}$$

when the layer is of infinite extent in the x-and z-directions (see Nield and Bejan 2006).

4 Asymptotic Analysis

Given that the critical values of S and a are 12 and 0, respectively, when the layer is horizontal, it is of interest in the first instance to determine how the critical value of S changes as the

inclination of the porous layer increases from zero as this may be determined analytically. We begin, therefore, with the perturbation equations 33 and 34 subject to the boundary conditions Eq. 35. The analytical solution for small values of a follows by assuming time-independent disturbances, i.e. $\lambda = 0$. The method we use is closely related to that which is summarised in Nield and Bejan (2006). We use the expansions,

$$(f, h, S) = \sum_{n=0}^{\infty} (f_n, h_n, S_n)\, a^n. \tag{37}$$

Upon substitution of Eq. 37 into Eqs. 33 and 34 we obtain the following equations and their solutions in turn.

At leading order we have,

$$h_0'' = 0, \qquad f_0'' = -i\ S_0\, h_0'\, \sin \Phi. \tag{38}$$

and hence the solutions are,

$$h_0 = 1, \qquad f_0 = 0. \tag{39}$$

The function h_0 could have taken any nonzero constant at this point, and therefore we have chosen unity for the sake of convenience.

At $O(a)$ the governing equation for h_1 is,

$$h_1'' = -i \left(y - \frac{1}{2} \right) S_0\ \sin \Phi, \tag{40}$$

for which the solutions are,

$$h_1' = -i \left(\frac{y^2 - y}{2} \right) S_0\ \sin \Phi, \quad h_1 = -i \left(\frac{y^3}{6} - \frac{y^2}{4} \right) S_0\ \sin \Phi. \tag{41}$$

We note that we have omitted the arbitrary constant when determining h_1 from h_1'; it is argued that any nonzero arbitrary constant arising at this point could be removed by redefining the value of h_0.

The equation for f_1 is,

$$f_1'' = -S_0\ \cos \Phi - \left(\frac{y^2 - y}{2} \right) S_0^2\ \sin^2 \Phi, \tag{42}$$

and the solution is

$$f_1 = -S_0\ \cos \Phi \left(\frac{y^2 - y}{2} \right) - \frac{S_0^2\ \sin^2 \Phi}{24} \left(y^4 - 2y^3 + y \right). \tag{43}$$

The equation for h_2 which arises at $O(a^2)$ is

$$h_2'' = 1 - i\ S_0\, h_1 \left(y - \frac{1}{2} \right) \sin \Phi - i\ S_1 \left(y - \frac{1}{2} \right) \sin \Phi - f_1. \tag{44}$$

After substitution for f_1 and h_1, Eq. 44 may be integrated and the first boundary condition, $h_2'(0) = 0$, is then applied. This yields

$$\begin{aligned} h_2' = 12\, y\, \big[& S_0^2\, y\, (5 - 10\, y + 15\, y^2 - 6\, y^3)\ \sin^2 \Phi - 20\, S_0\, y\, (3 - 2\, y) \cos \Phi \\ & + 240 + 120\, i\, S_1 (1 - y) \sin \Phi \big]. \end{aligned} \tag{45}$$

This expression must also satisfy $h_2'(1) = 0$, and therefore, S_0 must satisfy the equation,

$$S_0^2 \sin^2 \Phi - 5\, S_0 \cos \Phi + 60 = 0. \tag{46}$$

Hence,

$$S_0 = \frac{5 \cos \Phi \pm \left(25 \cos^2 \Phi - 240 \sin^2 \Phi\right)^{1/2}}{2 \sin^2 \Phi}. \tag{47}$$

It is clear that, for small values of Φ, the two possible values of S_0 are the following,

$$S_0 \sim \frac{5}{\Phi^2} \quad \text{or} \quad S_0 \sim 12, \tag{48}$$

the latter of which is the well-known value for the horizontal constant-heat-flux layer. Thus, the familiar single zero-wavenumber solution for the horizontal layer is joined by a second when inclinations are nonzero. From Eq. 47, the two solutions merge when,

$$\tan^2 \Phi = \frac{5}{48} \quad \Rightarrow \quad \Phi = 17.887413^\circ, \qquad S_0 = \frac{5 \cos \Phi}{2 \sin^2 \Phi} = 2\sqrt{159} \cong 25.219040. \tag{49}$$

This special value of Φ coincides with the threshold angle above which the first branch of instability disappears; this statement will be clarified later by reference to Fig. 2.

5 The Numerical Methods

From a purely numerical point of view, the main aim of the present work is the solution of Eqs. 33–35 to obtain either neutral curves or decrement spectra, i.e. the variation of $\Re(\lambda)$ with S. This was undertaken by reducing the system of equations and their boundary conditions to a matrix eigenvalue problem. Using a uniform distribution of N mesh points between $y = 0$ and $y = 1$, both inclusive, second order accurate finite difference approximations were used to transform Eqs. 33–34 to the following matrix vector equations,

$$M_1 \boldsymbol{f} = M_2 \boldsymbol{h}, \qquad M_3 \boldsymbol{h} + M_4 \boldsymbol{f} = \lambda \boldsymbol{h}, \tag{50}$$

where $\boldsymbol{f}$ and $\boldsymbol{h}$ are the vectors of f-values and h-values at all the grid points, and where M_1 to M_4 are matrices arising from the discretisation process. We note that a straightforward ficitious point technique has been used at $y = 0$ and $y = 1$ to satisfy the Neumann conditions for the temperature perturbations at those points. These equations may be rearranged into the form,

$$(M_3 + M_4 M_1^{-1} M_2)\boldsymbol{h} = \lambda \boldsymbol{h}, \tag{51}$$

which is a matrix eigenvalue problem for λ. This was solved using the NAG graphics library routine, `f02gbf`. We note that this procedure has also been used in Rees and Bassom (2000), Rees and Postelnicu (2001) and Rees and Tyvand (2009).

Other critical points such as minima and the detection of isola points were found by employing a fourth order Runge Kutta scheme coupled with a shooting method to solve the appropriate extended systems of equations which correspond to these critical points. Details of these extended systems may be found in Rees and Bassom (2000) and are therefore not reproduced here.

In our computations we used 30 intervals for the matrix-eigenvalue calculations, but the critical point calculations used 100 intervals. The former was sufficient to render good graphical accuracy, while the latter gave at least six significant figures of accuracy in all cases.

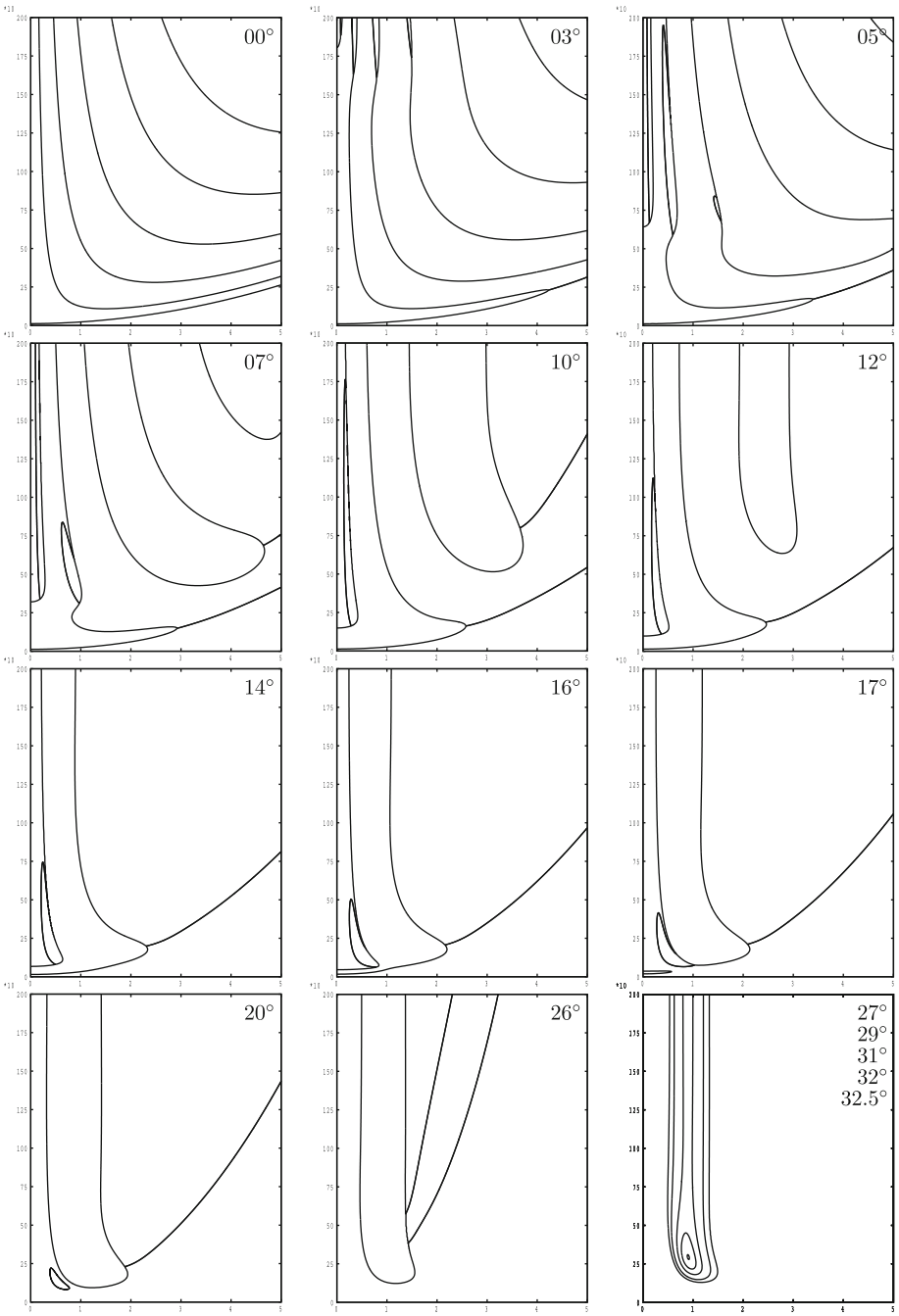

Fig. 2 Neutral curves for selected angles of inclination. The horizontal axis corresponds to $0 \leq a/\pi \leq 5$ while the vertical axis corresponds to $0 \leq S \leq 2000$

As a test for the absolute accuracy of the matrix eigenvalue scheme, we determined the two critical values of S which correspond to $a = 0$ when $\Phi = 12°$. The exact analytical values are given by Eq. 47 and are $S = 14.0006$ and $S = 99.1395$. The matrix eigenvalue solver yields values which are in error by 0.17% and 0.32%, respectively. Further tests were undertaken to match up the matrix eigenvalue solutions with the Runge-Kutta computations of various critical points (minima and isolae) and these too yield excellent comparisons.

6 Discussion of the Results

6.1 Neutral Curves

Figure 2 displays the neutral stability curves, namely S against a, for suitably chosen values of Φ. very many of the curves shown correspond to stationary modes, *i.e.* where $\Im(\lambda) = 0$, but some significant curves correspond to travelling modes where $\Im(\lambda) \neq 0$. These will be identified below.

When the layer is horizontal, $\Phi = 0°$, all the neutral curves correspond to the constant heat flux analogue of the Darcy–Bénard problem, and although they were all computed to be stationary modes, this fact may be confirmed by a simple demonstration that the linear stability equations are self-adjoint. For this inclination, Mode 1, the lowest mode, has its minimum at $S = 12$ and $a = 0$, as mentioned earlier.

As the inclination increases from zero, there are two general changes to the morphology of the $\Phi = 0$ neutral curves. The first is the merging of two neighbouring curves when a is sufficiently large. This may be seen at $S \simeq 230$ and $a/\pi \simeq 4.22$ when $\Phi = 3°$, for example, but two such mergings may also be seen when $\Phi = 10°$; these are called Type 1 travelling modes. The second is the formation of the vertically elongated loops, two complete examples of which may be seen when $\Phi = 5°$. In all cases, as one is travelling in the direction of increasing values of S along a stationary mode curve, then the travelling mode branch bifurcates to the left, and then reattaches from that side at a higher value of S. These are Type 2 travelling modes.

At slightly larger inclinations each of the latter type of travelling mode branches eventually becomes smaller and disappears. When $\Phi = 5°$ the loop on what is the mode 3 curve when the layer is horizontal is just about to disappear as Φ is increased further. This phenomenon appears to be a general feature of the evolution of the neutral curves with Φ. However, the one exception to this is the loop on the mode 2 branch which executes a different route to annihilation. As Φ increases from 15° the now last remaining loop becomes increasingly separate from the mode 2 curve. In the meantime the two stationary mode branches which have their minima at $a = 0$ join together and upper of these branches separates from the rest of the mode 2 branch. The newly coupled stationary modes shrink and disappear at $\Phi = 17.887413°$, as given in Eq. 49, after which there is a sudden jump in the critical value of S. Finally, the travelling mode loop detaches from its adjoining stationary mode branch to form a closed curve, and it then proceeds to diminish in size and disappear. This disappearance takes place at an isola point when $\Phi = 21.506827°$ at which $S = 123.999977$ and $a = 0.547538\pi$.

After this point a second travelling mode branch descends the right hand stationary branch, as seen for $\Phi = 26°$, and this latest loop eventually shrinks, disappears, and leaves the system with only stationary modes. Eventually the stationary modes themselves also disappear

via another isola point when $\Phi = 32.544793°$ and the corresponding values of S and a are $S = 293.254772$ and $a = 0.905772\pi$.

6.2 Decrement Spectra

Given that the evolution of the neutral curves with Φ is not straightforward, it is necessary to provide some explanation of how such complication arises. To this end we have chosen six cases and have created their decrement spectra, i.e. the variation of $\Re(\lambda)$ with S for fixed values of Φ and a. These are shown in Fig. 3; here we display stationary modes with a

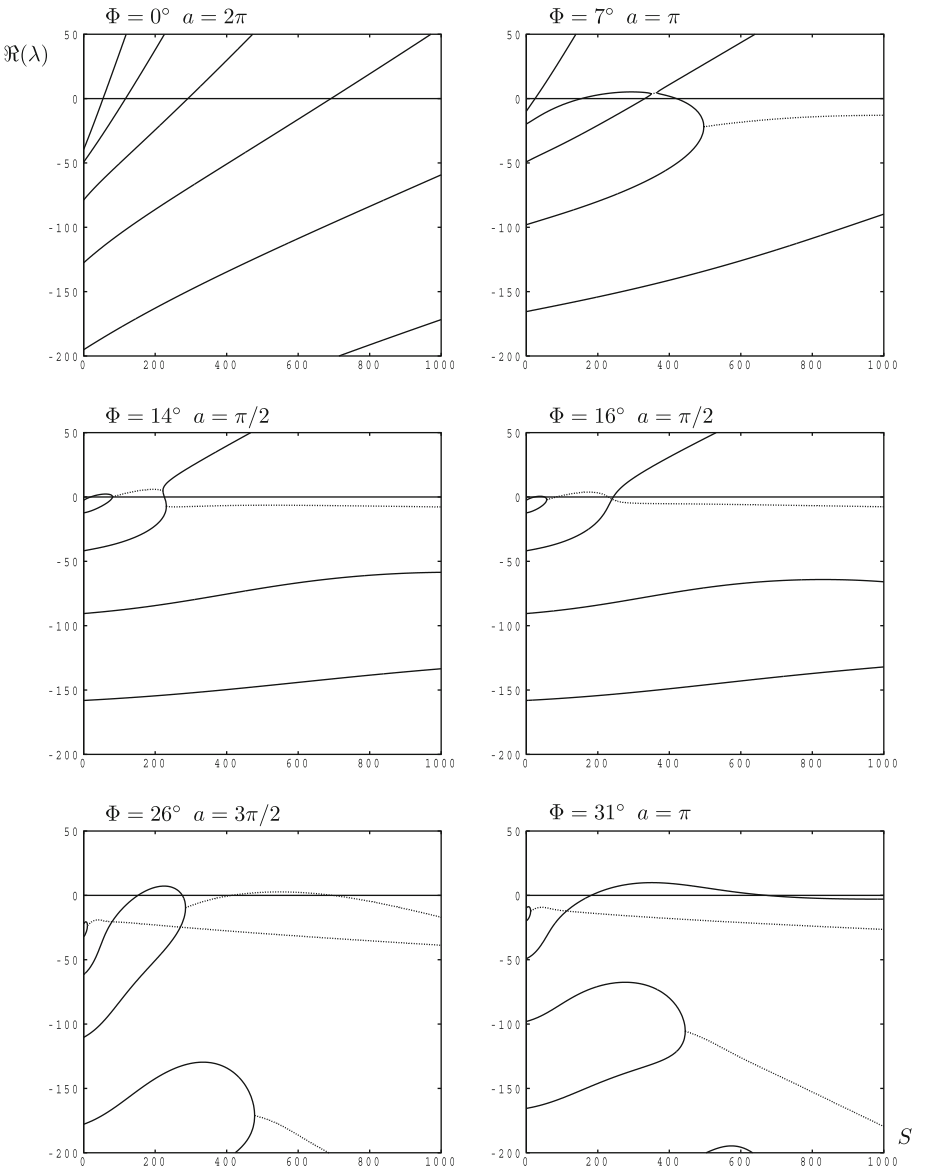

Fig. 3 Decrement spectra for selected inclinations and wavenumbers

continuous curve, while travelling modes correspond to dotted lines. For this subsection the mode numbers will refer to the order of the modes when $S = 0$ where mode 1 is the least stable mode.

The case, $\Phi = 0°$ and $a = 2\pi$, confirms our previous remark that modes are stationary when the layer is horizontal. Further, all modes are stable when S is sufficiently small, and the value of λ increases with S in all cases, so that all higher modes eventually become unstable.

When $\Phi = 7°$ and $a = \pi$ modes 2 and 4 eventually coalesce into a pair of travelling modes, the dotted line corresponding to both which are distinguished by having values of $\Im(\lambda)$ of opposite sign. However, there is also a very small range of values of S wherein modes 2 and 3 have merged into a pair of travelling modes, but they separate again very quickly.

The two cases for which $\Phi = 14°$ and $\Phi = 16°$ where $a = \pi/2$ depict a situation where an unusual transformation in the modal curves takes places as Φ increases. On numbering the modes as described above, modes 1 and 2 soon merge into a travelling mode pair, but then split again into stationary modes. In the meantime, the line corresponding to mode 3, a stationary mode, rises up to meet the newly split off mode 2 curve, and they subsequently merge to form a new travelling mode branch. In the figure, the curve which starts off as mode 3 takes an S-shape and eventually becomes mode 1. However, as Φ increases, the 'S' straightens out, allowing the two travelling mode curves to join together. The curves shown for $\Phi = 16°$ corresponds to just after this has taken place. Now the original mode 3 curve rises and eventually becomes the dominant mode, while modes 1 and 2 merge and thereafter maintain their identity as a pair of travelling modes. It is also of some interest to note that, for $\Phi = 16°$ and $a = \pi/2$, there are three intervals of stability. The second and third of these are very short, but they nevertheless exist.

When $\Phi = 26°$ and $a = 3\pi/2$, all six modes that are depicted merge in their turns pairwise to form travelling modes. However, it is only the second pair which yield instability at any point. The behaviour of the decrements may also be cross-correlated with the neutral curves shown in Fig. 2.

Finally, when $\Phi = 31°$ and $a = \pi$, the stationary modes merge in a different order, but mode 3 remains as a stationary mode and yields only a short interval of instability. Again, the effect of this on the shape of the neutral stability curves may be seen in Fig. 2.

6.3 Onset Criterion

Figure 4 shows the critical value, $S_{\rm cr}$, of the modified Darcy–Rayleigh number, Eq. 32, as a function of the angle Φ which have been obtained by minimising the value of S over all wavenumbers as Φ increases. Figure 5 shows the associated critical wavenumber, $a_{\rm cr}$. Figure 4 reveals that there are three main branches which, in turn, take over as being the most unstable. The first one, for small Φ, corresponds to the zero-wavenumber solution described by the asymptotic analysis given earlier. After the disappearance of the loop which is associated with the two zero-wavenumber solutions, there is a jump in the value of $S_{\rm cr}$ at $\Phi = 17.887413°$ from $S_{\rm cr} = 25.219049$ to $S_{\rm cr} = 68.52326$, which is a travelling wave branch. Then, at $\Phi = 21.153739°$ and $S_{\rm cr} = 99.147018$, there is a switch to a third branch of stationary modes. Finally, the maximum inclination for instability is $\Phi = 32.544793°$, at which point we have $S_{\rm cr} = 293.254772$ and $a_{\rm cr} = 0.905772\pi$. When $\Phi > 32.544793°$ the basic solution is linearly stable, although this does not preclude the possibility of large amplitude nonlinear solutions.

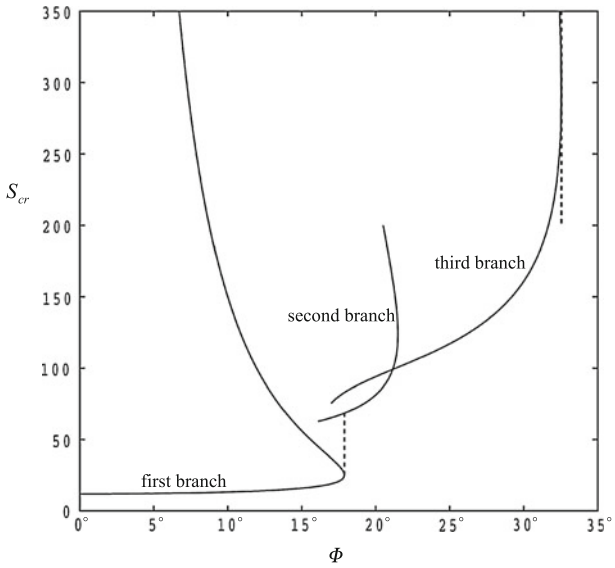

Fig. 4 Plot of S_{cr} versus Φ; the *dashed lines* denote the threshold angle above which the first branch of instability disappears, $\Phi = 17.887413°$, and the threshold angle above which no instability is possible, $\Phi = 32.544793°$

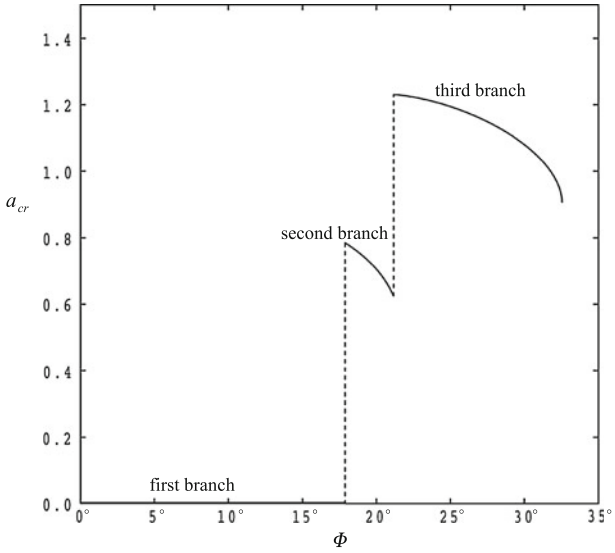

Fig. 5 Plot of a_{cr} versus Φ; the *dashed lines* denote the threshold angle above which the first branch of instability disappears, $\Phi = 17.887413°$, and the threshold angle above which the second branch becomes subdominant, $\Phi = 21.153739°$

7 Conclusions

In this paper we have presented a thorough analysis of the onset of convection in an inclined porous layer subject to constant heat flux boundary conditions. We have presented a sufficient number of neutral curves at chosen angles of inclination so that the manner in which the

neutral curves change with inclination can be understood. Decrement spectra for some chosen cases were also shown to understand more fully some aspects of the shapes of the neutral curves. Given that zero-wavenumber modes play an essential role at moderate inclinations, we have also provided a small-wavenumber asymptotic analysis.

These results were then summarised by showing the variation of the overall critical value of S and the minimising value of the wavenumber with inclination. There are three different regimes for the onset of convection. The zero-wavenumber mode is the favoured one when $\Phi < 17.887413°$, while an unsteady mode with a nonzero wavenumber dominates in the range $17.887413° < \Phi < 21.153739°$. Another steady mode, but one with nonzero wavenumber, then occupies the range, $21.153739° < \Phi < 32.544793°$, while the basic state is linearly stable at higher inclinations. This is in quite strong contrast to the analogous constant-temperature case studied by Rees and Bassom (2000), in which the preferred mode is always stationary and where there are no transitions between competing modes. For that paper, the maximum angle for which the basic state is unstable was found to be $\Phi = 31.49032°$, which is surprisingly close to the present value. Indeed, the final extinction of the steady mode as Φ increases displays very similarly-shaped neutral curves, and therefore it is possible that the extinction of linear stability is almost independent of the detailed boundary conditions that are imposed.

References

Bories, S.A., Combarnous, M.A.: Natural convection in a sloping porous layer. J. Fluid Mech. **57**, 63–79 (1973)

Horton, C.W., Rogers, F.T.: Convection currents in a porous medium. J. Appl. Phys. **16**, 367–370 (1945)

Kim, M.C., Lee, S.B., Kim, S., Chung, B.J.: Thermal instability of viscoelastic fluids in porous media. Int. J. Heat Mass Transf. **46**, 5065–5072 (2003)

Kimura, S., Vynnycky, M., Alavyoon, F.: Unicellular natural circulation in a shallow horizontal porous layer heated from below by a constant flux. J. Fluid Mech. **294**, 231–257 (1995)

Lapwood, E.R.: Convection of a fluid in a porous medium. Proc. Camb. Philos. Soc. **44**, 508–521 (1948)

Mamou, M., Mahidjiba, A., Vasseur, P., Robillard, L.: Onset of convection in an anisotropic porous medium heated from below by a constant heat flux. Int. Commun. Heat Mass Transf. **25**, 799–808 (1998)

Nield, D.A.: Onset of thermohaline convection in a porous medium. Water Resour. Res. **11**, 553–560 (1968)

Nield, D.A., Bejan, A.: Convection in Porous Media. 3rd edn. Springer-Verlag, New York (2006)

Rees, D.A.S.: The stability of Darcy-Bénard convection. In: Vafai, K., Hadim, H.A. (eds.) Handbook of Porous Media, Chapter 12, pp. 521–558. CRC Press, New York (2000)

Rees, D.A.S., Bassom, A.P.: Onset of Darcy-Bénard convection in an inclined layer heated from below. Acta Mech. **144**, 103–118 (2000)

Rees, D.A.S., Mojtabi, A.: The effect of conducting boundaries on weakly nonlinear Darcy-Bénard convection. Transp. Porous Med. (2011) doi:10.1007/s11242-011-9722-0

Rees, D.A.S., Postelnicu, A.: The onset of convection in an inclined anisotropic porous layer. Int. J. Heat Mass Transf. **44**, 4127–4138 (2001)

Rees, D.A.S., Tyvand, P.A.: Onset of convection in a porous layer with continuous periodic horizontal stratification. Part I. Two-dimensional convection. Transp. Porous Med. **77**, 187–205 (2009)

Riahi, N.: Nonlinear convection in a porous layer with finite conducting boundaries. J. Fluid Mech. **129**, 153–171 (1983)

Sen, M., Vasseur, P., Robillard, L.: Multiple steady states for unicellular natural convection in an inclined porous layer. Int. J. Heat Mass Transf. **30**, 2097–2113 (1987)

Tyvand, P.A.: Onset of Rayleigh-Bénard convection in porous bodies. In: Ingham, D.B., Pop, I. (eds.) Transport Phenomena in Porous Media II, Chapter 4, pp. 82–112. Pergamon, New York (2002)

Vasseur, P., Satish, M.G., Robillard, L.: Natural convection in a thin, inclined, porous layer exposed to a constant heat flux. Int. J. Heat Mass Transf. **30**, 537–549 (1987)